Tectonic inversion of salt-detached ramp-syncline basins as illustrated by analog modeling and kinematic restoration

Maria Roma[1], Oskar Vidal-Royo[2], Ken McClay[3], Oriol Ferrer[1], and Josep Anton Muñoz[1]

Abstract

Salt-detached ramp-syncline basins are developed in extensional settings and are characterized by wide synclinal sedimentary basins detached on salt and formed above the hanging wall of active ramp-flat-ramp extensional faults. They are rarely fault bounded; instead, they are bounded by salt structures that are in general parallel to the major subsalt structures. As such, the formation of these extensional systems requires the presence of (1) a subsalt extensional fault with significant dip changes and (2) an evaporitic unit above the extensional fault, which partially or completely decouples the basin from a subsalt extensional fault. Salt-detached ramp-syncline basins have a significant exploration potential when their extensional geometry is preserved and when they have undergone positive tectonic inversion and consequent uplift and fold amplification. However, in some cases, their subsalt geometry may not be fully recognizable, especially when subsalt seismic imaging is poor. To obtain a deeper understanding of the geometry and kinematic evolution of these salt-detached ramp-syncline basins, we performed a series of analog modeling experiments, in which the models' cross sections had been sequentially restored. Analog models and restoration results reveal that the kinematic evolution of the salt-detached ramp-syncline basins during extension and inversion depends on the interaction of different factors that may function simultaneously. Our results are used to improve the interpretation of seismic sections in inverted Mesozoic salt-detached ramp-syncline basins on the Atlantic margins, where subsalt faults are not well-imaged, and thus the suprasalt geometries must be used to infer the subsalt structure.

Introduction

Synclinal basins are defined as sedimentary basins that developed in the core of a syncline where synkinematic sediments are not bounded by major faults. Basins with synclinal geometries have been classically defined in contractional scenarios (e.g., piggy-back basins; Ori and Friend, 1984). Nevertheless, these basins can also develop via a range of mechanisms: (1) by extension above the hanging wall of active normal fault with dip variations (Figure 1a), (2) by salt evacuation (Figure 1b), or (3) by a combination of both (Figure 1c).

Synclinal basins may develop in the absence of salt when a ramp-flat-ramp extensional fault is involved; then a ramp-syncline basin is developed above its hanging wall (Figure 1a). The ramp synclines are characterized by asymmetric synclines with depocenters younging landward (McClay, 1990; Benedicto et al., 1999; Figure 1a). Where salt evacuation is the main mechanism controlling their growth, synclinal basins may develop as a consequence of sinking minibasins (Figure 1b). In this case, minibasins are small basins largely surrounded by salt walls and in the simplest cases, they contain vertically stacked depocenters (Jackson and Talbot, 1991; Rowan and Vendeville, 2006; Hudec et al., 2009; Callot et al., 2016; Figure 1b). Additionally, synclinal basins may also develop in hybrid systems (i.e., involving subsalt extensional faults and salt evacuation). In this scenario, when the extensional fault has a ramp-flat-ramp geometry, the resulting synclinal basin has been given numerous names: (1) extensional-ramp basins in Guimerà et al. (1995); (2) extensional hanging-wall syncline basins in Benedicto et al. (1999); and (3) hanging-wall synclinal basins in Ferrer et al. (2016) (Figure 1c). We propose that the term salt-detached ramp-syncline basin (Figure 1c) be used to describe all synclinal sedimentary basins that formed above active ramp-flat-ramp extensional faults and are detached on salt. In this case, the extensional salt tectonic system is characterized by (1) subsalt landward and basinward rollovers, (2) two wide salt-

[1]Universitat de Barcelona, Institut de Recerca GEOMODELS, Departament de Dinàmica de la Terra i de l'Oceà, Facultat de Ciències de la Terra, C/Martí i Franquès s/n, Barcelona, Spain. E-mail: mariaroma@ub.edu; joferrer@ub.edu; jamunoz@ub.edu.
[2]Terractiva Consulting SL, Barcelona, Spain. E-mail: oskar@terractiva.net.
[3]Royal Holloway University of London, Fault Dynamics Research Group, Earth Sciences Department, Egham, UK. E-mail: k.mcclay@rhul.ac.uk.
Manuscript received by the Editor 21 April 2017; revised manuscript received 8 September 2017; published ahead of production 02 November 2017; published online 21 December 2017. This paper appears in *Interpretation*, Vol. 6, No. 1 (February 2018); p. T127–T144, 12 FIGS., 1 TABLE.
http://dx.doi.org/10.1190/INT-2017-0073.1.

detached ramp-syncline basins, not bounded by normal faults but by salt-cored anticlines, and (3) the trend of the basins and bordering salt structures are generally parallel to the major subsalt structures (Figure 1c). However, if the amount of extension and decoupling is significant, the basin can be transported away from the subsalt fault ramp to above a subsalt fault flat (Carola, et al., 2015). Clearly, salt-detached ramp-syncline basins differ from the typical extensional minibasins because salt-detached ramp synclines can be a hundred times wider and the subsalt fault geometry is the main factor controlling these sedimentary basins, with or without the presence of salt. The salt acts as an effective décollement decoupling subsalt and suprasalt deformation (Vendeville, 1987, 1988; Koyi and Petersen, 1993; Nalpas and Brun, 1993; Vendeville et al., 1995; Steward and Clark, 1999; Withjack and Callaway, 2000; Ferrer et al., 2016), but such scenarios follow a partial coupling structural style, where the salt unit acts as a thin-skinned component in a thick-skinned deformation style. The basement fault does not penetrate the salt unit but is overlain by a draped fold over the master fault (Jackson and Hudec, 2017).

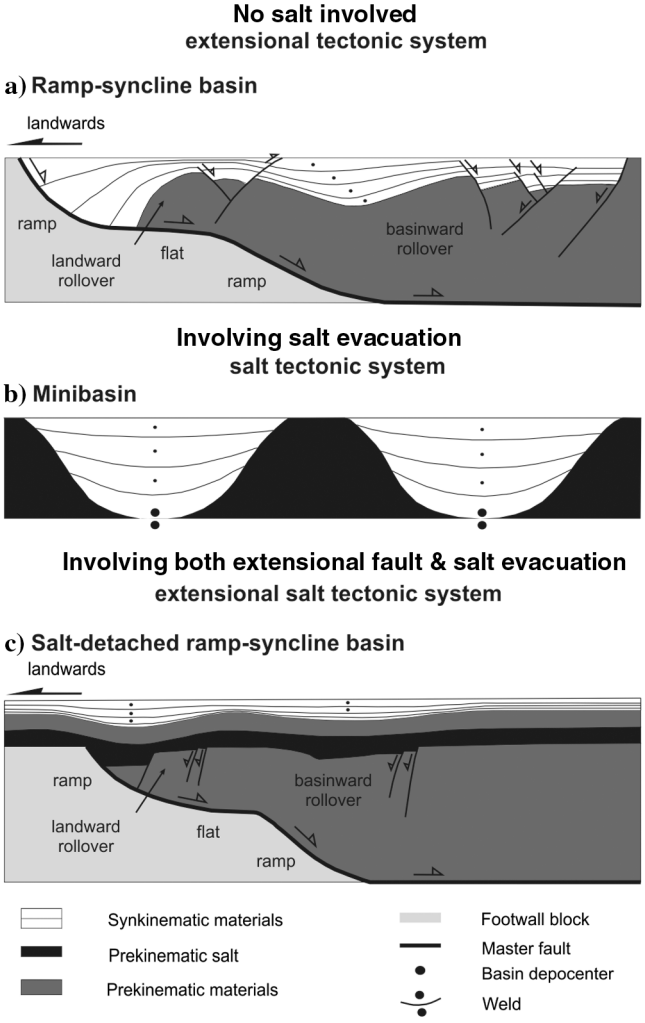

Figure 1. Conceptual models of (a) a ramp syncline developed in a salt-free extensional tectonic system, modified from McClay (1990), (b) a minibasin developed in a a salt tectonic system, and (c) a salt-detached ramp-syncline basin developed in an extensional salt tectonic system, modified from Ferrer et al. (2016).

Mesozoic extensional basins around western Europe, as well as in their equivalent North-American Atlantic margin, are characterized by synclinal geometries detached from subsalt faults by Late Triassic (Keuper and Dagorda) or Permian (Zechstein) evaporites, e.g., Parentis Basin (Ferrer et al., 2012, see Figure 2), Sogne Basin (Stewart and Clark, 1999), Jeanne d'Arc Basin (Tankard et al., 1989), Orpheus Basin (Withjack and Schlische, 2005), and the Lusitanian Basin (Alves et al., 2002). In these basins, the salt was deposited at the late stages of extensional deformation related to the breakup of Pangea during Permo-Triassic times (Coward, 1995; Glennie, 1995). As a result, the interaction between the subsalt fault structure and the main synrift depocenters is characterized by multiple rift events with deposition of salt during and after the extensional phase (Ziegler, 1988; Balkwill and Legall, 1989; Tankard et al., 1989; Dercourt et al., 1993; Rasmussen et al., 1998; Jackson et al., 2000; Alves et al., 2002). Consequently, the salt shows lateral variations in thickness (Jackson and Vendeville, 1994; Coward and Steward, 1995; Ferrer et al., 2008, 2014; Rowan, 2014). Furthermore, most of these basins were subsequently partially or totally tectonically inverted during the Late Cretaceous – Cenozoic, e.g., Parentis (Mathieu, 1986) or Lusitanian Basins (Alves et al., 2002) or incorporated into a fold-and-thrust belt, e.g., the Organyà (Muñoz, 1992) and Cameros Basins (Guimerà et al., 1995). Further complicating matters, the distribution and thickness of the evaporitic unit as well as the inherited structure at the end of the extensional phase determined the structural style during tectonic inversion of the mentioned examples. The complexity of this resulting geologic scenario together with the poor quality of the available seismic data, often hinder precise interpretation of subsalt data, and they consequently obscure the origin and kinematic development of the inverted basin. The use of scaled analog modeling allows reproducing an approximation of a natural geologic process. Thus, analog modeling can help in constraining the interpretation of the subsalt data, understanding the interaction between the subsalt fault and the evaporites during the extensional phase, and understanding the overprinted tectonic inversion phase.

For the past 80 years, analog modeling has been used to understand these complex geologic systems. For example, Roure et al. (1992) and McClay (1990) use a prekinematic sand pack (an analog of brittle materials in nature) over a rigid wooden footwall block and a plastic sheet (used to reproduce the fault geometry and fault motion) to study the formation of ramp synclines. Soto et al. (2007) and Ferrer et al. (2014) follow the previous technique, and they use different fault geometries — listric, ramp-flat listric, planar, and kinked — but they also tested the role of a shallow

prekinematic polymer layer (as an analog of salt in nature) within the brittle sand pack to simulate salt-detached ramp-syncline basins. More recently, Ferrer et al. (2014) consider a synkinematic ductile layer. Furthermore, McClay (1989), Buchanan and McClay (1991), and Yamada and McClay (2003) use different techniques to previously extend the model and then reverse the direction of motion to produce the subsequent inversion. Only the recent work of Durcanin (2009) and Ferrer et al. (2016) considers the inversion phase, including a polymer layer in the prekinematic configuration. They note the control of the inherited salt configuration and salt structures during inversion. But, they do not especially address it in large amounts of extension and inversion phases, in multiple rift events, in salt kinematics, and how salt influences the resulting structural style.

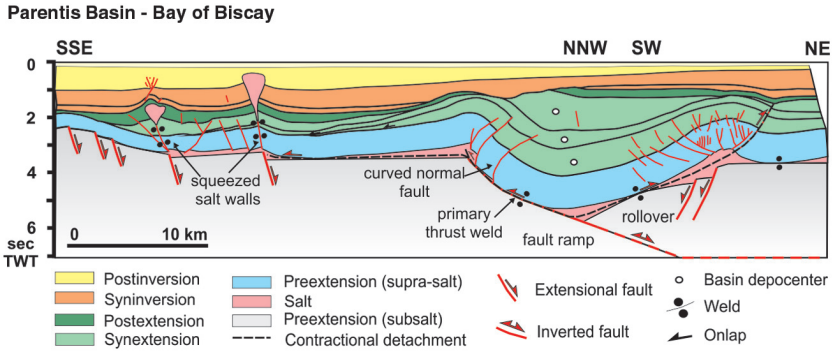

Figure 2. Natural example of an inverted salt-detached ramp-syncline basin. Line drawing of a seismic section of the inverted Parentis Basin (Bay of Biscay) with a prekinematic salt unit. Modified from Ferrer et al. (2012).

We have supplemented the works by Durcanin (2009) and Ferrer et al. (2016) by investigating the results of two analog models of salt-detached ramp-syncline basins developed above a ramp-flat-ramp rigid wooden footwall block. The models underwent two phases of extension with synkinematic salt deposited between them, and they were subsequently deformed by later inversion. We analyzed two representative sections across the model, illustrating domains with and without well-developed diapirism. The cross sections were then sequentially restored with geometric algorithms to illustrate the structural evolution as well as the variations in sectional area of the salt.

The experimental results are consistent with the interpretation of Ferrer et al. (2012) on the Parentis Basins (Figure 2), and they also lead to a new interpretation of the Lusitanian Basin, modifying the previous one by Alves et al. (2002). As such, our results can serve as a guide for improving the interpretation of seismic lines in other salt basins, where these styles of extensional salt tectonics develop.

Modeling methodology

Two experiments are presented in this paper. Both experiments simulate polyphase deformation. In detail, the models were initially extended by 7 cm, at which point our salt analog (silicone polymer) was added and followed by a further 8 cm of extension (15 cm of total extension). Experiment 1 was terminated at the end of the two extensional phases, whereas experiment 2 was inverted by 8 cm of shortening after the end of extension.

Experimental setup

The experimental setup was similar to that used by Yamada and McClay (2003) and Ferrer et al. (2016). The analog models were carried out in a 63 cm long, 30 cm wide, and 35 cm deep glass-sided deformation box (Figure 3a). A rigid wooden block with four kinked

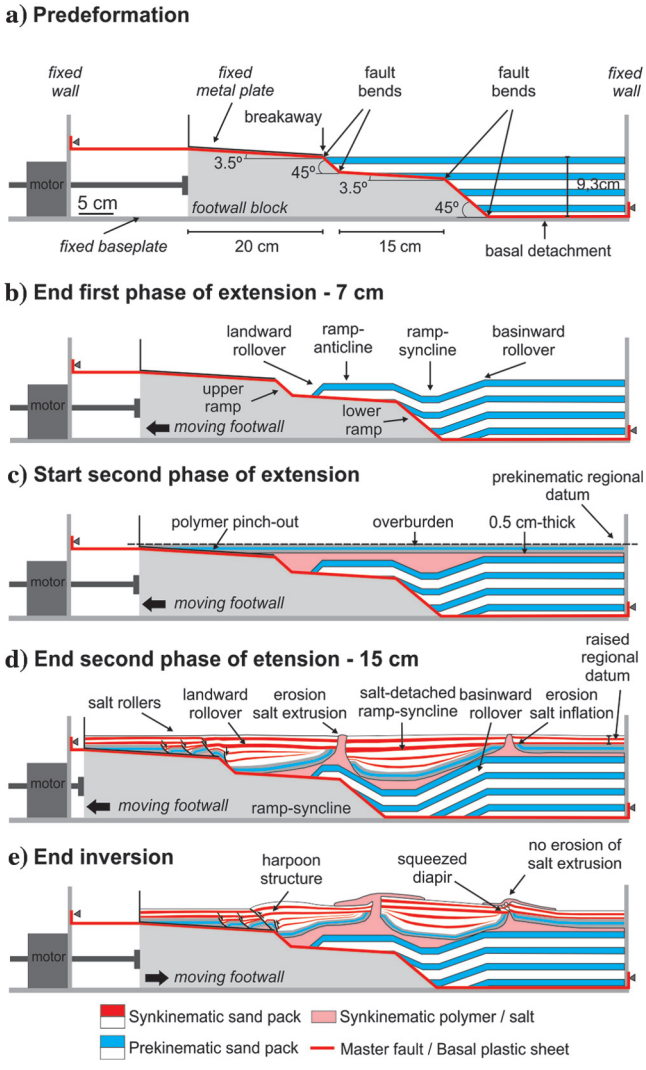

Figure 3. Simplified sketch illustrating the experimental apparatus: (a) predeformation geometry, (b) configuration of the experiments 1 and 2 at the end of first phase of extension — 7 cm, (c) experimental configuration prior to the second phase of extension for experiments 1 and 2, (d) configuration of the experiments 1 and 2 at the end of second phase of extension — 15 cm, and (e) configuration of the experiment 2 at the end of the inversion.

fault bends was used as a footwall geometry that imposed a ramp-flat-ramp geometry to the master fault. Both ramps dip at 45°, and they were separated by two panels dipping at 3.5° with an adjacent horizontal basal detachment at the base of the model (Figure 3a). We placed a plastic sheet above the footwall block to reproduce the master fault motion (Figure 3a, solid red line). The plastic sheet remained attached at both end walls during extension and inversion. We fixed a metal plate above the upper footwall flat to form the breakaway fault (Figure 3a); here, the plastic sheet went underneath the metal plate. Extension was achieved by pulling the footwall block away using a motor-driven worm screw (Figure 3d). For the inversion of experiment 2, the motion of the footwall block was reversed to produce contraction of the hanging wall section (Figure 3e).

Modeling materials

The materials used in the experimental program (Table 1) were well-sorted, subrounded dry silica sand and polydimethylsiloxane (PDMS) polymer. The dry sand was chosen to simulate the brittle deformation of upper crustal sedimentary rocks (Horsfield, 1977; McClay, 1990), and the PDMS polymer was used as our salt analog (Weijermars, 1986), as in most analog modeling studies (Koyi et al., 1993; Nalpas and Brun, 1993; Vendeville et al., 1995; Withjack and Callaway, 2000; Dooley et al., 2005; Soto et al., 2007; Ferrer et al., 2014, 2016). Silica sand has a Mohr-Coulomb behavior at moderate values of normal stress, and its mechanical properties were measured using a ring shear tester at the Fault Dynamics Research Group Laboratory. The poured dry sand had an average grain size of 250 μm, an angle of internal friction of 34.6°, a bulk density of 1500 $kg \cdot m^{-3}$, and a low apparent cohesive strength of 55 Pa. The polymer (PDMS) has a near-perfect Newtonian fluid behavior when deformed at a laboratory strain rate of 1.83×10^{-4} $cm \cdot s^{-1}$ (Weijermars, 1986). It has an effective viscosity of 1.6×10^4 $Pa \cdot s$ and a density of 972 $kg \cdot m^{-3}$ at 20°C. The coefficient of sliding friction between the plastic sheet and the sand pack was 0.37 (Huiqi et al., 1992).

Table 1. Scaling parameters used in the experimental program.

Quantity	Experiment	Nature	Model/nature
Length, L (m)	0.01	1000	10^{-5}
Density loose sand, ρ ($kg \cdot m^3$)	1500	2700	0.55
Gravity acceleration, g ($m \cdot s^{-2}$)	9.8	9.8	1
Angle of internal friction, φ (°)	34.6	40	0.87
Cohesion loose sand, σ (Pa)	55	10^7	5.5×10^{-6}
Density polymer, ρ ($kg \cdot m^3$)	972	2200	0.44
Viscosity, η (Pa·s)	1.6×10^4	10^{18}–10^{19}	$1.6 \times 10^{-14/-15}$

The experiments were geometrically, kinematically, and dynamically scaled (e.g., Hubbert, 1937; Schellart, 2000), such that with a length ratio of 10^{-5}, 1 cm in the model corresponds to approximately 1 km in nature (Table 1).

Experimental procedure

The layered prekinematic sand pack for both models was formed by pouring 3 mm thick, horizontal white and colored sand layers into the deformation box using a mechanical scraper. This prekinematic unit covered the entire model with a total thickness of 9.3 cm above the horizontal basal detachment (Figure 3a). The models were initially extended 7 cm at a displacement rate of 1 cm per 10 min. No synkinematic strata were added during this first phase of extension (Figure 3b). The accommodation space was then infilled by a polymer showing important variable thickness (Figure 3c). The polymer has a horizontal upper surface, a thickness of 0.5 cm on the right section of the model, and it pinches out on the upper footwall flat. The polymer was covered by a 1 cm thick sand layer prior to the second phase of extension (overburden in Figure 3c).

The second 8 cm of extension (15 cm in total) was applied to both models at a rate of 1 cm per hour (Figure 3d). During this phase, synkinematic layers were added by pouring alternating layers of red, white, and black sand after every 0.5 cm of extension, keeping the prekinematic regional datum constant (Figure 3c). The models were paused for 15 min during the deposition of each second extensional phase synkinematic sand layer. Any topographic highs that had formed by polymer inflation were eroded during the synkinematic layering (Figure 3d), thus removing the overburden and enhancing subsequent polymer rise. When the polymer reaches the surface of the model on these inflated areas, the regional datum was raised by 3 mm for each subsequent synkinematic layer, thus simulating the passive growth of the salt wall (Figure 3d). Any polymer surface extrusion was manually removed with a sharpened knife (it has only removed the entire polymer overhang without affecting the diapir stem) during the second phase of extension (simulating salt dissolution and erosion in nature) before adding a new synkinematic layer (Figure 3d). The polymer surface extrusions are also removed to avoid Christmas-tree structures (repeated salt extrusion over the underlying strata, which create stacked salt wings forming a serrated contact). Removing the polymer extrusion, we simplify the extensional geometry of the salt structures and we also reduce the complexity of the subsequent inverted salt structures.

Experiment 2 followed the same procedure as experiment 1, but was in-

verted 8 cm after the end of the second phase of extension (Figure 3e) at a shortening rate of 1 cm per hour, until reaching the null point of the second extensional phase. Nonerosion and synkinematic layers were added during the inversion phase.

At the end of both experiments, the models were covered by a thick postkinematic sand layer to preserve the final topography and to inhibit any undesired movement of the polymer. Then, the models were preserved and serially sectioned at a spacing of 0.3 cm.

The tops and the sides of the models were recorded by high-resolution digital time-lapse photography. The final cross sections were also recorded using digital photography.

Restoration procedure

Two final cross sections of experiment 2 were sequentially restored to illustrate the structural evolution of the two main domains across areas with well-developed salt walls and across areas without extruded salt walls. The sequential restoration shows (1) the change in basin geometry due to extension, positive inversion, and diapirism, and it highlights the different responses to deformation of the subsalt and suprasalt units and (2) the variations in the area of the salt section between the subsalt and suprasalt units at each phase.

The subpolymer and suprapolymer units in the analog models were restored independently using different strain transformations (i.e., restoration methods) for each. The suprapolymer deformation is characterized by folding and faulting as a consequence of extension and compression — triggering polymer mobilization — and therefore flexural slip, unfolding to a known datum (regional) was applied, allowing conservation of the line length and area (Dahlstrom, 1969; Groshong et al., 2012; Lingrey and Vidal-Royo, 2015). The deformation of the subpolymer sand pack was generated by slip along the master fault, and was restored using the fault parallel flow algorithm in Move by applying the measured fault offsets between consecutive restoration phases.

Modeling limitations

The main limitation of our experimental setup is that the rigid footwall block that constrains the geometry of the extensional fault (Figures 4 and 5) prevented the formation of basement-involved footwall shortcuts and horses, as in Nalpas et al. (1995) and in Eisenstadt and Sims (2005). Besides, higher friction between the glass-side walls and the polymer/sand pack produced a border effect on the structures (Ferrer et al., 2016). As a consequence, there was preferred polymer inflation at the central part of the model during the second extensional phase. In addition, the polymer produces smearing against the glass side walls, which obscures the detailed evolution of structures at these phases. Consequently, the evolution of the models was determined by the analysis of vertical cross sections at the end of the experiments and their sequential restoration combined with overhead time-lapse photographs. The restored sections in Figures 6 and 7 show differences in restored line lengths between the subpolymer and suprapolymer units. To explain the differential line length, the actual geologic processes that have been described in nature and are replicated by sandbox models include (1) internal shear and readjustment of particles because of the ongoing deformation regime; and (2) out-of-section movement due to salt tectonics and transpression (Casas et al., 1996; Koyi, 2000; Koyi and Sans, 2006; Burberry, 2015). Consequently, we consider internal shear as the main factor to take into account when it comes to considering bed length and area conservation in the restoration of compressional structures. During the analysis of the cross sections and the overhead photographs, we omitted a 3 cm wide section to avoid the border effects.

Modeling results

Experiment 1 and 2 — Two phases of extension

The results of the first and second extensional phases can be seen in experiments 1 and 2.

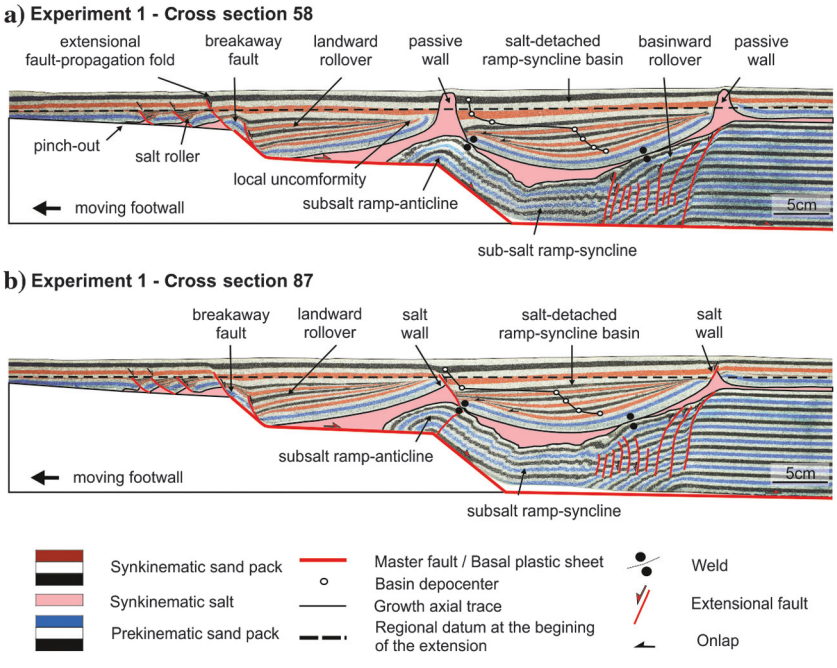

Figure 4. Interpreted cross section of the structures observed in experiments 1 and 2 at the end of the second phase of extension (after 15 cm of lengthening) and with the terminology used in this paper. (a) Cross section 58 and (b) cross section 87. The location of the cross sections is shown in Figure 5.

First phase: 0–7 cm of extension

The first phase of extension produced translation of the prekinematic strata over the master fault, which generated fault-related folding of the hanging wall (Figure 3b). This formed a landward rollover, together with a fault-bend fold ramp anticline and a ramp syncline over the major footwall ramp. In addition, a basinward rollover anticline formed where the master fault flattened out into the horizontal basal detachment on the right side of the model (Figure 3b). Minor antithetic normal faults developed within this large rollover panel. All these structures were covered by a salt unit (i.e., polymer) of variable thickness at the end of the first extensional phase (Figure 3c).

Second phase: 7–15 cm of extension

The second phase of the extension reactivated the main master fault. The subsalt structures developed during the first phase of extension are still recognized during the entire second phase of extension (Figure 4). The width of the subsalt ramp anticline decrease as the extension progressed; in contrast, the subsalt ramp syncline was amplified as a result (Figure 4). With continued extension, an extensional forced fold developed at the breakaway fault (Figures 5a, 6b, and 7b), evolving into an extensional fault-propagation fold (Figures 4a, 6c, and 7c). During this process, the salt thinned above the upper ramp favoring the upward propagation of this fault into the synextensional sand pack (Figures 4 and 6c). Once subsalt and suprasalt units were completely coupled, a curved normal fault nucleated on the upper ramp (Figure 5b). At the early stages of the second phase of extension, several small listric faults with triangular footwall salt rollers were formed in the upper footwall flat to the left of the breakaway (Figures 4 and 5a).

Upward fault propagation was inhibited, where the salt was the thickest (above the lower ramp). Continued extension was accommodated by the formation of a salt-detached ramp-syncline basin lying above the salt unit and above the subsalt ramp syncline (Figures 4, 6c, and 7c). The lithostatic load produced by synkinematic sedimentation — combined with the subsalt fault slip — triggered salt flow from the areas with high vertical load (basin depocenter) to the edges of the salt-detached ramp-syncline basin, where the vertical load was lower (e.g., Kehle, 1988; Koyi et al., 1993; Hudec and Jackson, 2007; Ferrer et al., 2014). This gave rise to salt-inflated areas bounding the salt-detached ramp syncline (Figure 7c). The erosion of salt-inflated areas (local unconformity in Figures 4 and 6d) above the regional datum (Figure 5a), as well as the effective decoupling of subsalt and suprasalt materials, favored the growth of reactive (Figure 6b) to passive salt walls (Figure 6e) at the edges of the salt-detached ramp-syncline basin (Figure 4a and 4b). The salt walls only pierced the cover in the center and along the glass-side walls of the experiment (cross section 58, Figures 4a, 5a, and 6f). The continuity of the source layer was interrupted after the formation of basin welds gave rise to coupled deformation near the end of the extensional phase (Figures 4 and 6f).

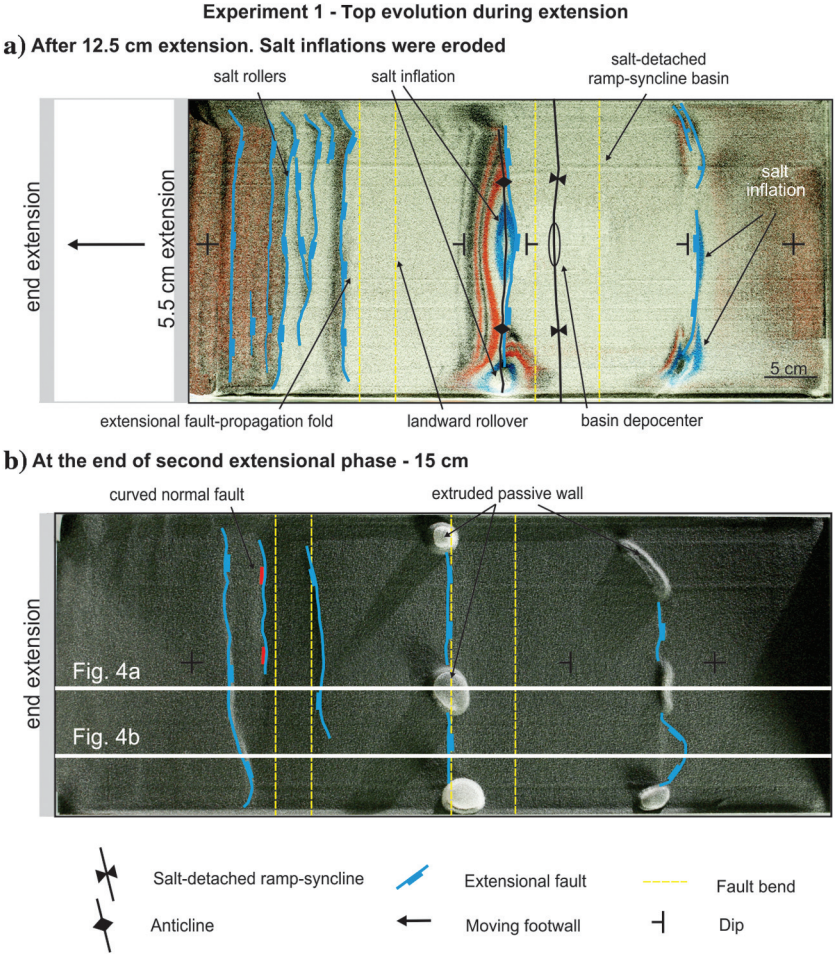

Figure 5. Interpreted overhead photographs illustrating the structural evolution of experiments 1 and 2 during extension. (a) After 12.5 cm extension and (b) at the end of the extension (15 cm total), the horizontal white lines indicate the location of the experiment 1 cross sections in Figure 4.

Experiment 2 — Two phases of extension followed by inversion

Figure 8 shows the result of 8 cm of bulk shortening superimposed on two phases of extension similar to those described in experiment 1. Inversion produced the reactivation of the master fault and the salt flow. Both cross sections in Figure 8 show a broad frontal harpoon structure (see Buchanan and McClay, 1991) formed by contractional

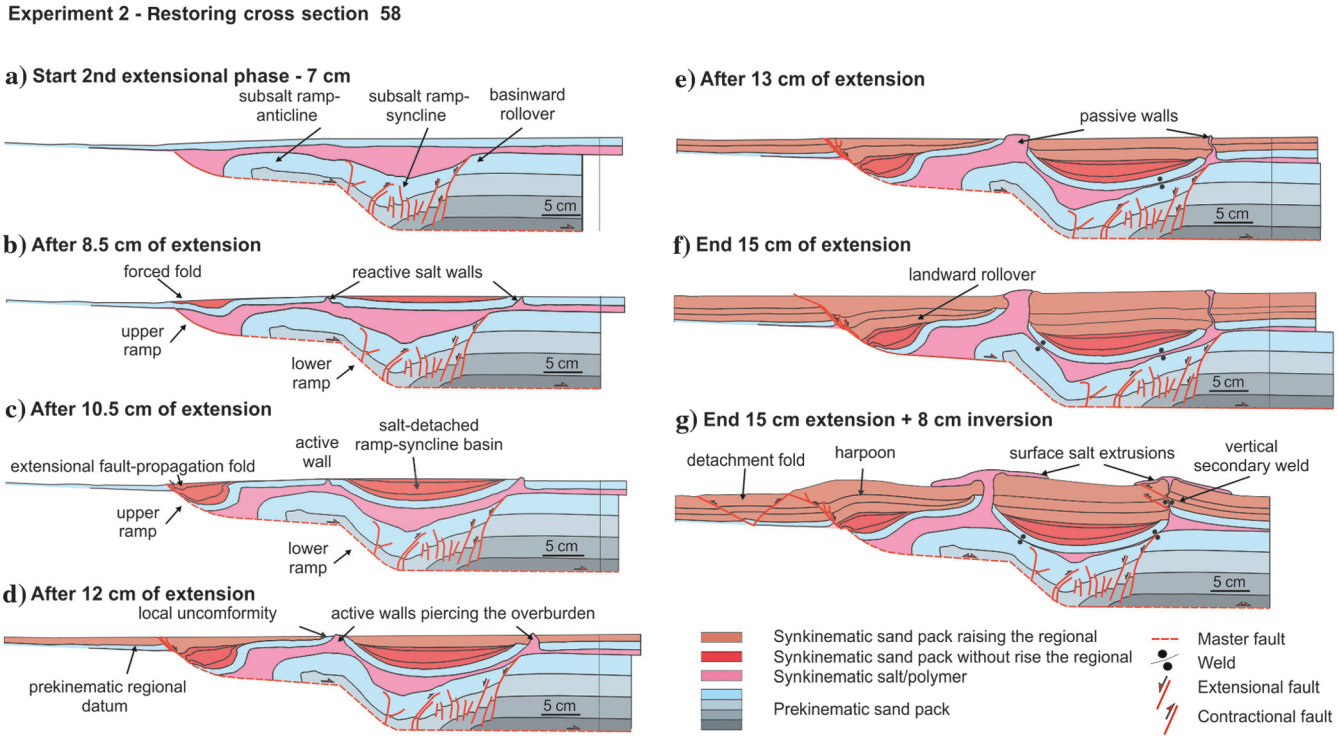

Figure 6. Sequential restoration of cross section 58 from experiment 2 illustrating the structural evolution during the second phase of extension. (a) Prior to the second phase of extension where is shown the subsalt structures developed during the first phase of extension; (b) after 8.5 cm of extension, there is suprasalt forced fold above the upper ramp and two reactive salt walls developed at both basin edges; (c) after 10.5 cm of extension, the suprasalt forced fold become an extensional fault-propagation fold and the reactive salt wall become an active salt wall; (d) after 12 cm of extension, the active salt walls pierced the overburden and consequently the prekinematic regional datum was raised; (e) after 13 cm of extension, the active salt walls become passive; (f) after 15 cm of extension, the salt-detached ramp syncline has already welded against the subsalt structures; and (g) at the end of 8 cm of inversion — net contraction with regard to the second phase of extension.

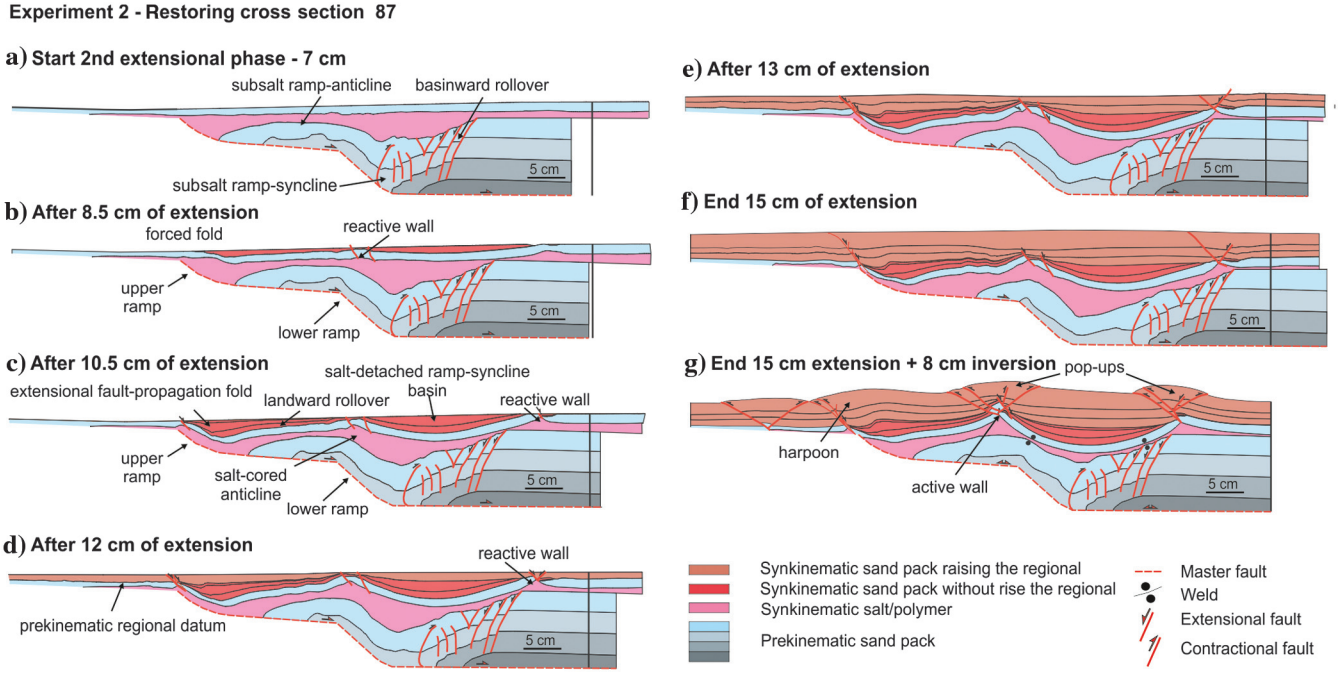

Figure 7. Sequential restoration of cross section 87 from experiment 2 illustrating the structural evolution during the second phase of extension. (a) Prior to the second phase of extension; (b) after 8.5 cm of extension, a suprasalt forced fold and a reactive salt wall were developed; (c) after 10.5 cm of extension, the suprasalt forced fold become an extensional fault-propagation fold; (d) after 12 cm of extension, the prekinematic regional datum was raised; (e) after 13 cm of extension; (f) after 15 cm of extension; and (g) at the end of 8 cm of inversion — net contraction regard to the second phase of extension.

reactivation of the breakaway fault (structure 1 in Figure 9a). In the footwall of the harpoon structure, minor displacement at the base of the thin salt resulted in a small amplitude faulted detachment fold (Figure 8 and structures 7 and 9 in Figure 9c). The subsalt ramp anticline and ramp syncline in the prekinematic units were pushed back up along the master fault (Figure 8a and 8b). The salt-detached ramp-syncline basin was welded against the subsalt structures during the inversion phase and became rapidly uplifted, tightened, and narrowed during the inversion. At the end of extension, the weld surfaces at both syncline limbs were narrow and local (Figure 4). In contrast, at the same point at the end of the inversion (Figure 8), the joining area of the welds increases. The inherited salt wall, above the basinward rollover, at the end of extension was squeezed shut with the consequent development of secondary welds and the formation of a thrust at the salt wall pedestal (Rowan and Vendeville, 2006; Dooley et al., 2015) (Figure 8a). At this point, subsalt and suprasalt deformations became coupled. In contrast, the left side polymer walls were squeezed, thereby forcing salt extrusion, but not the development of secondary welds.

The top surface of experiment 2 constrains the temporal evolution of the inversion phase (Figure 9). The first phase of contraction reactivated the breakaway fault resulting in the frontal harpoon fold and thrust (structure 1 in Figure 9a). The squeezing of the inherited salt walls increased salt extrusion at this phase of shortening. Continued shortening produced more uplift and folding, together with elongate-shaped salt-surface extrusions (Figure 9b). The formation of secondary welds at approximately 7–8 cm of shortening is indicated by a broad uplift above the regional datum (Figures 8, 9c, and 9d) and the formation of thrusts (Figures 8a and 9d) that nucleated at the top of the salt wall pedestals.

Discussion

The analog models presented in this paper have successfully simulated the evolution of partial coupling models during the two extension and subsequent inversion phases.

Interaction of factors during the extensional phase

In the illustrated analog models, the salt distribution after the first extensional phase relies on the steepened geometry of the subsalt fault. During the second extensional phase, the degree of decoupling between subsalt and suprasalt units and the salt withdrawal due to sediment loading mainly depends on salt thickness (e.g., Koyi and Petersen, 1993; Koyi et al., 1993; Vendeville et al., 1995; Richardson et al., 2005). Although a thinner salt unit promotes the development of extensional fault-propagation folds and premature welds by salt depletion, a thicker salt unit allows a partially coupled deformation, which results in further salt migration and the development of wide salt-detached ramp-syncline basins (Figure 4). Synkinematic sediment loading triggered salt expulsion that contributed to the development of the wide salt-detached ramp-syncline bounded by salt walls.

Some salt rollers also developed detached on the thin salt unit (Figure 4) because (1) the salt flows toward the space created by the upper ramp and (2) the basinward tilt of the footwall flat promotes gravitational gliding.

The final salt-detached ramp-syncline basin depocenters are laterally shifted toward the ramp anticline (see the growth axial trace formed by the shifted depocenters dipping basinward in Figure 4). This markedly differs from the salt distribution and stratal geometry associated with extensional forced folds (Withjack and Callaway, 2000; Tavani et al., 2013; Tavani and Granado, 2014), whereby they are characterized by wide monoclines with often vertically stacked depocenters, and where the salt walls are only developed at the monocline hinge. Moreover, the basinward rollover structure present in the salt-detached ramp syncline does not exist in extensional forced folds.

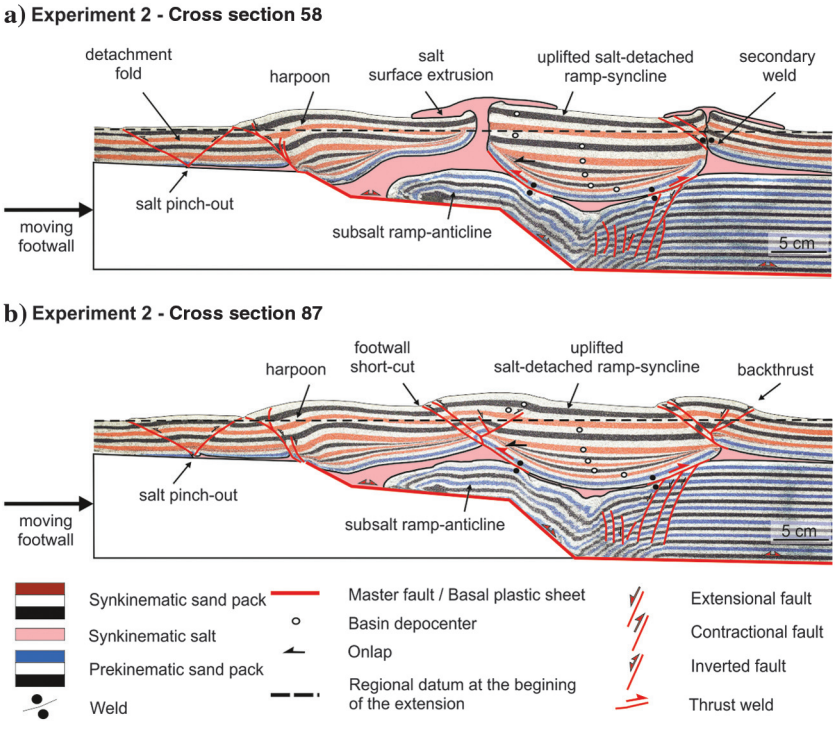

Figure 8. Interpreted cross section of the structures observed in experiment 2 at the end of the inversion (after two phases of extension followed by 8 cm of contraction) and with the terminology used in this paper. (a) Cross section 58 and (b) cross section 87. The location of cross sections is shown in Figure 9.

The growth axial trace (formed by the lateral stacking depocenters) dipping basinward is the result of the displacement of the synclinal basin from the lower ramp to the horizontal basal detachment (as occurs in McClay [1990]; see Figure 1a). In our models, such displacement was coeval with salt withdrawal, which is being preferentially expelled toward the adjacent left side salt wall (Figure 4a). This preferential migration promotes the decrease of the dip of the growth axial trace (Figure 4). During extension, the salt-detached ramp-syncline basin was tilted landward and some onlap geometries were formed (Figure 4). Both features observed together mean that there is a thin-skinned component and the main salt-detached ramp-syncline basin was decoupled and horizontally translated above the salt. Our models also show that in the shallowest synkinematic layers of the salt-detached ramp syncline, the depocenters appear totally shifted from the previous path (Figure 4a and 4b). This means that the salt-detached ramp-syncline basin becomes coupled with subsalt structures, and this occurs when welds form at the syncline limbs where salt is expelled, and the salt layer is exhausted (Figure 4).

Overall, in our models, we can observe through the synkinematic architecture, the interaction of four factors during extension: (1) the subsalt fault geometry and fault displacement, (2) the initial thickness of the salt unit and its distribution, (3) the salt withdrawal due to sediment loading, and (4) the degree of coupling between subsalt and suprasalt units (Ellis and McClay, 1988; Koyi et al., 1993; Withjack and Callaway, 2000). When the influence of one of those factors is dominant, the other factors may stay masked; e.g., the fault displacement is masked by salt migration when the synrift depocenters appear vertically stacked in salt-detached ramp-syncline basins (Figure 1c). Deciphering the contribution of each factor relies on the recognition of the stacking pattern of the depocenters and the stratal geometries within the synkinematic unit.

Role of salt during inversion phase

Most of the literature of analog models with rigid footwalls subject to inversion does not contemplate the presence of viscous detachments. Only the works of Durcanin (2009) (synextension polymer on the hanging wall of a listric fault) or Ferrer et al. (2016) (preextension polymer covering the entire models with different faults geometries) analyzed the role of salt during inversion using rigid footwalls. These authors pointed that subsalt and suprasalt contractional deformation could be partially coupled or completely decoupled depending on the inherited polymer configuration and the presence of primary welds at the beginning of the inversion. They also denote that preexisting salt structures (diapirs and walls) preferentially absorb contractional deformation during early inversion. The analog models presented in this manuscript, with more extension and inversion, support these statements, but also illustrate the salt kinematics during inversion and how salt influences the resulting structural style.

Despite the ductile layer, the inversion of the landward rollover was totally coupled (Figure 8), being similar to those described by Buchanan and McClay (1991) using isotropic models without a ductile layer. In this

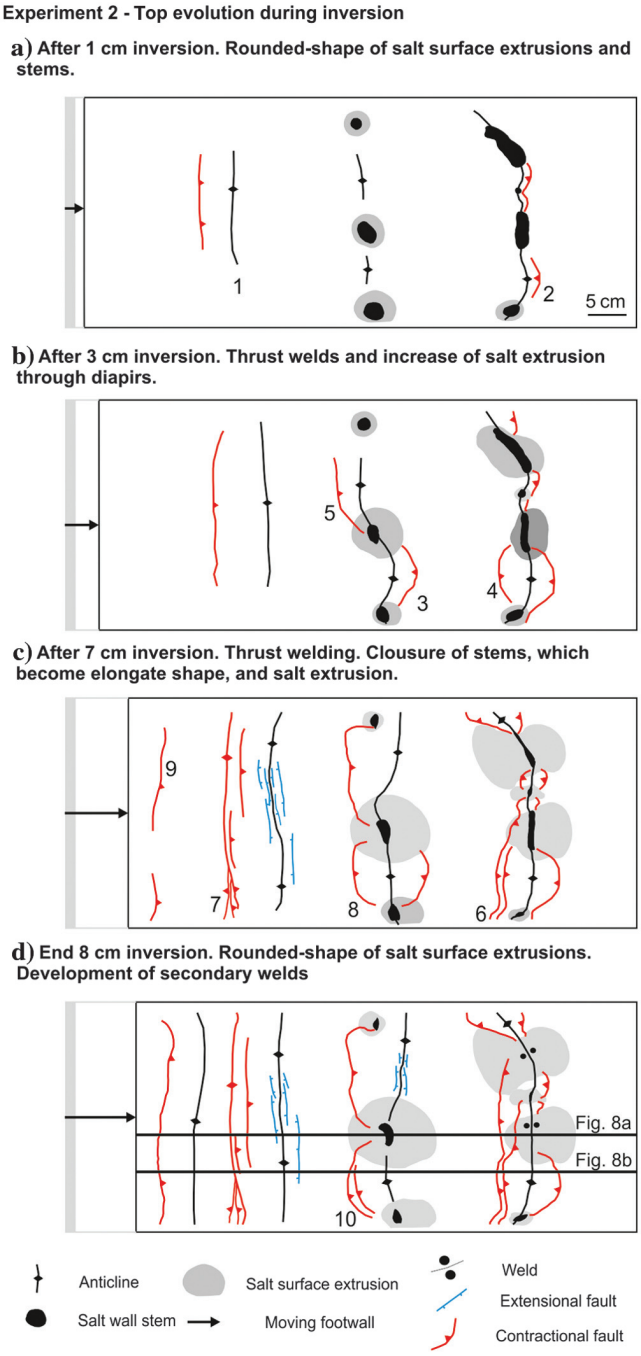

Figure 9. Interpreted overhead photographs illustrating the structural evolution of experiment 2 during the inversion: (a) after 1 cm of inversion, (b) after 3 cm of inversion, (c) after 7 cm of inversion, and (d) at the end of the inversion. The solid black line indicates the location of experiment 2 cross sections in Figure 8.

case, the master fault reactivation produced basin uplift with the development of a harpoon structure (Figure 6g). The upper ramp of the master fault propagated as a thrust into the synextensional sand pack. In the central part of the models, the presence of primary welds at the beginning of the inversion disrupts the source layer and prevents salt withdrawal from the salt-detached ramp-syncline depocenter toward the preexisting salt walls (Figure 4a). At this point, the system becomes wholly coupled and the up-slip contractional displacement of the subsalt unit along the lower ramp of the master fault is transferred into the suprasalt unit uplifting, tilting, and rotating clockwise the salt-detached ramp-syncline basin (Figure 8a). The inversion of the subsalt unit entails a progressive width lessening of the subsalt ramp syncline related to the draping of the sand pack over the master fault geometry and salt evacuation out of section (compare Figure 6f and 6g). As a consequence, primary welds are contractionally reactivated as thrust welds. This primary thrust weld has not been described previously in any natural case; e.g., in Rowan et al. (1999), a thrust weld will develop from a secondary weld. This reactivation implies an increasing of the welded area with respect to the beginning of the inversion (compare Figures 4a and 8a). In regions where salt structures are well-developed, these primary thrust welds transmit the shortening to the inherited passive salt walls that are progressively squeezed triggering salt extrusion (Figures 8a, 9b, and 9c). Despite that both salt walls are squeezed, only the one located above the basinward rollover hinge (Figure 4a) develops a secondary weld (Figure 8a). This is related to the 3D geometry and size of the welded area, larger and wider above the basinward rollover than in the ramp anticline. Whereas the salt wall located above the ramp anticline was fed by out-of-section polymer during inversion, the larger weld of the basinward rollover sector hampered out-of-section salt migration to feed the other salt wall during inversion (Figure 9c). Although the sections with reactive salt walls (Figure 8b) show slight differences in comparison with the previous ones, the regional structure after inversion is relatively similar with coupled deformation due to the inherited primary welds (Figure 4b). In a similar way, the basins developed as a consequence of the upper and lower ramps were progressively uplifted and tilted during inversion. Despite the absence of salt structures piercing the suprasalt sand-pack confining the salt (Figure 8b), the progressive loss of salt volume during inversion (Figure 10) indicates out-of-section salt migration. This difference in salt volume feeds the squeezed salt walls at the central part of the model during inversion (see the following section for more details). The reactive diapirs inherited from the extensional phase are preferentially deformed as the shortening propagates. Different thrust faults nucleate at the apex of the reactive diapirs developing an imbricate thrust system detached at the viscous layer (Figure 8b). The normal faults that controlled the growth of these reactive diapirs during the extension were involved in the hanging wall of these thrusts.

As occurs during extension, the interaction of different factors during inversion is also evident: (1) the subsalt fault geometry and fault displacement, (2) the inherited salt configuration, (3) the presence and geometry of preexisting salt structures, (4) the salt migration, and (5) the degree of coupling between subsalt and suprasalt units. In our models, these factors may function simultaneously. The subsalt master fault geometry and displacement are the main factors controlling the inversion phase in our models, also because the system is partially coupled by the welds. However, those fac-

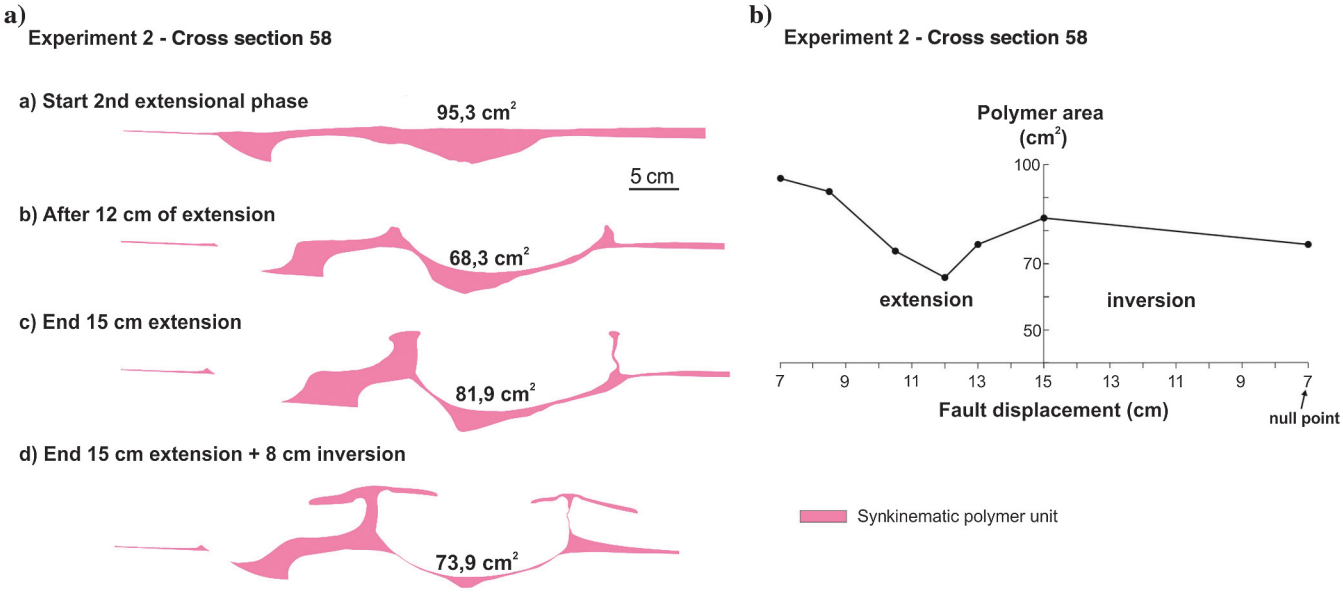

Figure 10. (a) Restoration of polymer area for section 58 from experiment 2 and (b) plot of polymer area versus fault displacement during extension (left side of the graph) and inversion (right side of the graph).

tors were coeval with the basin translation above the primary thrust welds, the reactivation of the salt structures and also the shortening accommodation toward the salt pinch-out, whereby denotes that the salt unit was reactivated.

Salt mobilization

The evolution in geometry and volume (the area in the section plane) of the salt is strictly related to the formation (or lack) of pierced salt walls in the model. Figures 10 and 11 illustrate the variation of salt area through extension and shortening for sections 58 and 87, respectively. The estimated initial polymer area on each section should be approximately 98.5 cm^2, assuming that the initial 2773 cm^3 volume of polymer was evenly distributed over the 30 cm wide, homogeneously folded, prekinematic units.

With the onset of the second phase of extension in section 58 (the central section of the model) (Figure 10a), the main subsided part of the salt-detached ramp-syncline basin caused a progressive loss of salt (Figure 10b). Due to border effects, we can determine that the basin geometry is almost conical (Figure 5a) (i.e., noncylindrical); therefore, the basin depocenter coincides with the central part of the model (Figures 4a and 5a from cross section 58). As a consequence, the salt tends to migrate radially. In this central section 58, the area of available salt reached its minimum at 12 cm of extension, losing approximately 28.3% (27 cm^2) of the salt in the form of out-of-section salt mobilization (Figure 10b); it coincided with the end of the reactive diapirism and also with the onset of passive diapirism. At 12 cm of the second extensional phase, the triangular shapes (reactive diapirsm) become open salt walls (passive diapirism), and they grow in width and height. At the end of this second extensional phase (15 cm), the area of available salt has increased by a total of 19.9% (13.6 cm^2 — including all material lost by the effects of extrusion and erosion, which corresponds to 455 cm^3 or 16% of the initial volume of salt volume lost through diapirs during the second extensional phase) (Figure 10c). This value indicates a large volume of salt that mobilized along-strike into the central section from the neighbouring areas (from Figure 11c to 10c). Finally, after the inversion of the basin, the salt area went out of the section, which resulted in a decrease of 8.7% (8 cm^2) (Figure 10d). This area of variation is surprisingly low. At this stage (Figure 10d), we would expect to quantify a great loss of salt because (1) the surface of joining primary welds was increased, (2) the formation of secondary welds, and (3) the large amount of salt being extruded. However, the key to understanding the small variation in salt volume in section 58 lies in the neighboring cross section 87 (Figure 11). At this particular stage, there is a large decrease in the salt area where no extrusion takes place (Figure 11d): from 98.9 cm^2 at the end of the second extensional event (Figure 11c), down to 50.8 cm^2 of salt available at the end of the compressional phase (Figure 11d). The difference totals up to 48.6% of the salt area lost (48.1 cm^2) during the inversion of the basin. This indicates that during the extension and inversion phases, a large volume of salt migrates across the model from outer areas (cross section 87, Figures 8b and 11) toward the central parts (cross section 58, Figures 8a and 10) of the model to feed the piercing salt walls. Beyond this, we can observe how the regions without diapirs, welds, and salt extrusion (cross section 87, Figures 8b and 11) are at the end of the regions that have lost more salt volume.

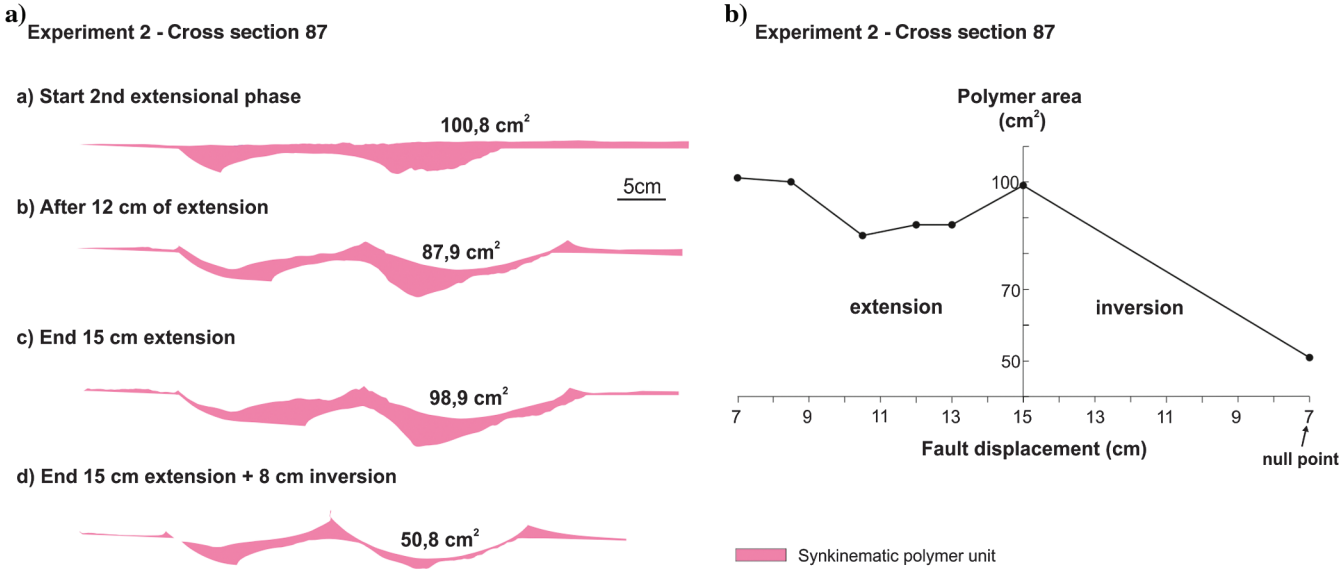

Figure 11. (a) Restoration of polymer area through the extension and inversion phases for section 87 from experiment 2 and (b) plot of the polymer area versus fault displacement during extension (left side of the graph) and inversion (right side of the graph).

Comparison between the analog model results and a natural example (Parentis Basin, Bay of Biscay)

The Parentis Basin (Figure 2) is a clear and published example of a salt-detached ramp-syncline basin, and our experimental results show some similar structural features and kinematic evolution. Although, Ferrer et al. (2014) try to support their interpretation using analog models, they only contemplate the evolution of the models during the extensional episode, without taking into account the Late Cretaceous-Middle Miocene inversion of the Parentis Basin. The analog experimental program of Ferrer et al. (2016) tests the influence of the inversion phase. However, they apply lesser extension than the calculated in the Parentis Basin. In this sense, our experiments include two large extensional phases with salt deposited between them and the later contractional episode, elucidating the role of the inherited extensional structure and salt during inversion.

The Parentis Basin (Figure 2) in the eastern Bay of Biscay is a moderately inverted extensional basin (Tugend et al., 2014) developed above a flat-ramp-flat fault with a Late Triassic salt unit (Keuper facies) in the lower part of the synrift sequence (Ferrer et al., 2012). The salt unit was deposited between the extensional deformation related to the Permo-Triassic breakup of Pangea and the main Early Cretaceous extension of the Bay of Biscay (Ziegler, 1988; Dercourt et al., 1993; Rowan, 2014). During the main rift phase (Early Cretaceous), the salt partially decouples the subsalt and suprasalt structures. In a similar manner to our experiments, the migration of the salt forced by thick-skinned extension led to the development of a wide salt-detached ramp syncline bounded by salt-cored anticlines and with similar laterally stacked depocenters formed in experiment 1. Actually, the Parentis Basin is welded above the hanging wall rollover panel and the footwall fault ramp (Figure 2); in contrast, in our experiments (Figure 4) the salt-detached ramp syncline is welded during the extensional phase against the subsalt ramp anticline and the basinward rollover (compare the location of the primary welds between the case study and experiment 1 in Figures 2 and 4, respectively). In the Parentis Basin, Ferrer et al. (2012) do not interpreted a subsalt ramp anticline, but eventually in our models, the process that developed the landward rollover (welded against the upper ramp) together with the salt-detached ramp syncline, could explain the structures observed in the Parentis Basin. The evolution of the models suggests that the development of welds in the Parentis Basin have been done during the extension phase and not during inversion. In the Parentis Basin, welding at the fault ramp (Figure 2) forced the development of curved normal faults and modified the trend of the synextensional depocenter path (Figure 2). Similar curved normal faults can be observed detached on the upper ramp in experiment 1 during the extensional phase (Figures 4a and 5b).

In the eastern Parentis Basin (Figure 2), the salt-cored anticlines bounding the basin did not become piercing diapirs. This disagreement between our models result and the Parentis Basin is related to (1) the thickness of the prekinematic overburden (Withjack and Callaway, 2000), (2) the effect of the erosion, and (3) the synextension sediment supply. First, in the Parentis Basin, the suprasalt prekinematic isopach layer (unit blue in Figure 2) is thicker than the prekinematic overburden in our experiments (Figure 3c). Second, in the Parentis Basin, the synkinematic materials raise the prekinematic regional datum at the beginning of the extension, whereas, in our models, the regional datum was raised after the diapirs pierced the cover. Third, the interpreted seismic section of the Parentis Basin does not show any erosion during the extensional phase at both salt-cored anticlines. Contrarily, in our models, we can observe an important unconformity generated by the erosion of the salt inflations (Figures 4a and 5a). This thinner cover and the erosion are the principal mechanisms triggering the piercing salt walls in our analog models (Coward and Stewart, 1995).

Later, the ongoing Pyrenean shortening during Late Cretaceous to Middle Miocene times produced contractional reactivation of the subsalt extensional fault that resulted in the uplift of the Parentis Basin. The presence of a major Late Cretaceous unconformity on the top of the basin infill denotes that the Parentis Basin was tectonically inverted. During this episode, the Parentis Basin was slightly inverted compared with other basins located further south, which were incorporated into the Pyrenean orogeny.

Unfortunately, our models do not include erosion during inversion phase; therefore, we are not able to test changes in the kinematic evolution and in the uplift of the basin due to erosion effect (Konstantinovskaya and Malavieille, 2011). However, similar processes have been done in analog experiment 2 and the Parentis Basin. In experiment 2 (Figure 8) and the Parentis Basin (Figure 2), the salt-layer configuration, at the onset of the inversion phase, appears offset (without continuity) by the welds. Nevertheless, our models show that shortening produces the contractional reactivation of the source layer through the primary thrust welds. A similar process could occur in the Parentis Basin, giving rise to the contraction of the basin-bounding salt-cored anticlines (Figure 2). The Parentis Basin also shows that squeezed salt walls developed above the footwall fault (Figure 2), whereas in experiment 2, there are well-developed detachment folds detached at the salt pinch-out (Figures 8a and 9d). These structures are also the result of the reactivation of the salt layer as a contractional detachment above the footwall master fault (Figures 2 and 8).

Our model results provide insights into the processes that can explain the geometries observed in Ferrer et al. (2012), and the previous comparison lends support to their work.

Analog model application to improving seismic interpretation (Northern Lusitanian Basin, offshore Portugal)

The northern Lusitanian Basin is a good example of a basin developed via hybrid thick- and thin-skinned structural styles during extension and subsequent inversion, but the available seismic imaging data in this salt-bearing region are quite poor. This occurs because seismic waves refract when passing between media having different velocities (salt usually has a higher P-wave velocity than the surrounding sediments) (Jackson and Hudec, 2017). A wavefront passing through salt encased in sediments is distorted at the top and the base of the salt before reflecting off subsalt units and distorting further if returning to receivers through the salt. Seismic processing attempts to unscramble this returning wave to produce a coherent image of the subsalt section. However, limitations in seismic acquisition may still leave a poor subsalt image (Jackson and Hudec, 2017). In this sense, although the suprasalt and shallow structures are well-characterized, the interpretation of the subsalt structures are problematic and make it difficult to understand the origin and kinematic evolution of salt-bearing basins. In fact, the analog modeling provides one of the most powerful and visual tool to understand the 4D structural evolution as well as providing possible poorly imaged geometries of the subsalt basins in seismic data.

Although the suprasalt geometry of the Lusitanian Basin published by Alves et al. (2002) is comparable with our experimental results, the subsalt interpretation could be improved. However, according to the processes and control factors that our analog models demonstrate in relation to the coupling-decoupling between the subsalt and suprasalt structures, the use of suprasalt features obtained in analog results can help to constrain the subsalt fault geometry and provide an alternative kinematic evolution of the Lusitanian Basin.

The Lusitanian Basin (Figure 12a) is related to the rifting that led to the breakup of Iberia and northeastern North America (Alves et al., 2002). Multiple rift events, from Late Triassic to Early Cretaceous, were developed (Stapel et al., 1996; Jackson et al., 1998) with the deposition of the Dagorda salt Formation during the Late Triassic. Subsequently, the second Late Jurassic rift phase was the main triggering event for salt tectonics. Where the salt was thin, subsalt faults propagated into suprasalt units and promoted the development of extensional forced folds and fault-propagation folds (compare the analog models of Figure 4 with the seismic sections published by Alves et al. [2002], notably, their Figure 3). However, where the salt was thick, subsalt and suprasalt deformation was partially decoupled, as well as the suprasalt and subsalt interpretation (Figure 12a). It is at this point where the subsalt extensional master faults could be misinterpreted. Together with the original interpretation by Alves et al. (2002) (Figure 12a), we are providing a new interpretation (Figure 12b), based on what the analog models show. In this last scenario, where the salt was thick, the statements of Alves et al. (2002) (Figure 12a) do not fit with the extensional forced fold analog models published by Withjack and Callaway (2000) for two reasons. First, its synclinal geometry and, second, the developed onlaps (Figure 12a and 12b) require a thin-skinned deformation style with significant horizontal displacement of the suprasalt units above the subsalt fault steps — similar to the models presented in this paper. Furthermore, the synclinal geometry in Figure 12a had been interpreted by Alves et al. (2002) as the result of salt withdrawal. However, our experimental results indicate that the development of the salt-detached ramp-syncline basin was mainly controlled by the geometry of the subsalt fault (Figure 12b), similar to our models (ramp-flat-ramp). The decoupling effect of the salt is also revealed by the thin-skinned structural style of the Lusitanian Basin during the Miocene inversion, which is related to Pyrenean-Alpine shortening. Our experimental results suggest that the salt-cored anticlines nucleated on inherited salt structures (from the second phase of extension) during the Miocene inversion (compare the analog models of Figure 4 with the seismic sections published by Alves et al. [2002], in our Figure 12a). Alves et al. (2002)

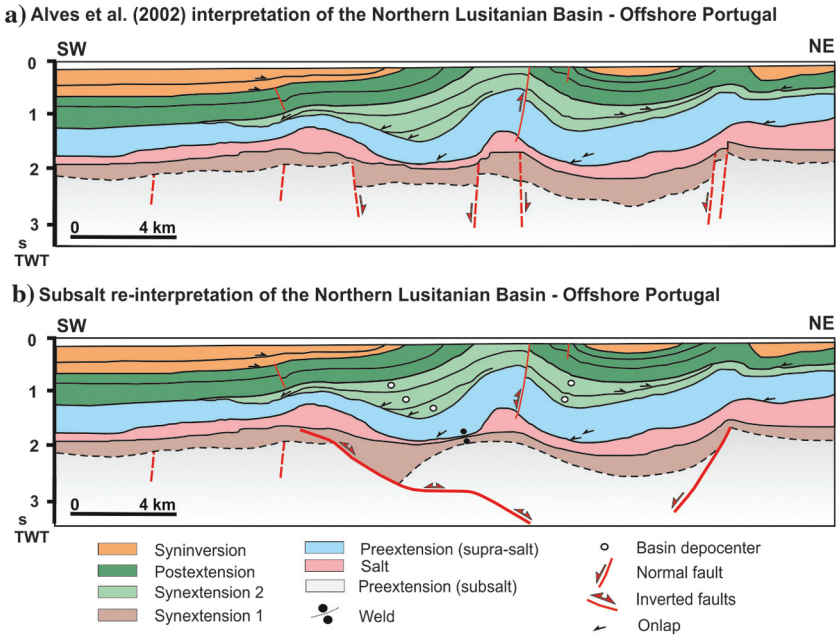

Figure 12. (a) Interpreted seismic line S84-23, modified from Alves et al. (2002), of the Northern Lusitanian Basin (offshore Portugal) containing synstretching salt according to Rowan (2014) and subsequent pronounced period of inversion according to Alves et al. (2002) and (b) reinterpretation of the subsalt structure of seismic line S84-23 from Alves et al. (2002) in the northern Lusitanian Basin (offshore Portugal).

say that the Lusitanian Basin was resolved by a thin-skinned structural style during inversion, as evidenced by the seismic data, but the subsalt faults were interpreted by Alves et al. (2002) following a thick-skinned style, and according to the structural relief shown by the sedimentary basin, as explained by high-angle subsalt faults underneath the salt.

Therefore, the suprasalt deformation patterns resemble those observed in our model results. In this sense, we offer an alternative interpretation based on the insights found in the subsalt and suprasalt deformation coupling in the analog models. Therefore, new constraints for the interpretation of subsalt extensional master fault were presented in this paper (Figure 12b).

Conclusion

Our physical models illustrate the role of salt during the development of salt-detached ramp-syncline basins in areas that have undergone multiple rifting events and subsequent inversion. Therefore, the analog results can be useful (1) to support published interpretations where geometries similar to the ones in our models can be observed, (2) assist in the reinterpretation of seismic sections in subsalt areas where imaging is problematic, and (3) serve as a guide for other similar salt basins.

The experimental results at the end of the extension reveal that suprasalt hanging wall structures are controlled by the interaction of (1) the subsalt fault geometry and fault displacement, (2) the initial thickness of the salt unit and its distribution, (3) salt withdrawal, and (iv) the degree of coupling between the subsalt and suprasalt units. The ramp-flat-ramp subsalt fault constrained three variables: the development of the ramp-syncline basin related to the concave-up fault bend during the first extensional phase, the thickness of the salt layer after the first extensional phase, and the salt flow during the second subsequent extensional phase. The variable salt thickness akin to its synrift nature promotes decoupling between suprasalt and subsalt units, with the development of wide salt-detached ramp-syncline basins when the salt is thicker. This is similar to what was observed on the development of the Parentis Basin in the eastern Bay of Biscay, the Matelles, and Ales Basins in the Gulf of Lion, the Angola passive margin, West Africa, and the Nordkapp Basin. In contrast, early extensional forced folds evolving to extensional fault-propagation folds develop when the salt is thinner, thus favoring coupled deformation and the upward propagation of subsalt faults. Equivalent structures have been interpreted in the Lusitanian Basin, offshore Portugal, the Stavenger fault system in North Sea, and in the central Suez rift or the Haltenbanken area in offshore Norway. The interaction between the extension rate, basin subsidence, salt withdrawal, and decoupling between the subsalt and suprasalt units enhances the development of salt ridges and walls at the edges of the salt-detached ramp-syncline basin. They also constrain the stacking pattern of synrift depocenters and stratal geometries in the basin.

The interaction of different factors during inversion is also evident in analog models and natural examples: (1) the subsalt fault geometry and fault displacement, (2) the inherited extensional structure and salt configuration, (3) the presence and geometry of preexisting salt structures, (4) the salt migration, and (5) the degree of coupling between subsalt and suprasalt units. The subsalt faults were inverted, thereby forcing the arching and uplift of suprasalt units along with the development of harpoon structures, or the uplifting and tilting of the salt-detached ramp syncline. Despite the ductile layer, the presence of primary welds at the beginning of the inversion disrupts the source layer and the system becomes completely coupled. Nevertheless, shortening promotes the squeezing of the salt structures and at passive walls increases the salt extrusion rate (see the Essaouira Basin, the western Atlas system). We highlight that our analog model results show that during the uplift of the cover, some primary welds are contractionally reactivated as thrust welds, transferring the contractional deformation to the suprasalt unit. This has not been described in any natural case. The restoration of some cross sections also illustrates the along-strike salt migration to feed the extruded salt bodies. When these salt structures are squeezed shut, vertical secondary welds develop and vergent thrusts nucleate at the salt pedestal (e.g., in the Loberbus diapir, northwestern Tunisia and in thrusted diapirs from offshore Angola). This contractional evolution is consistent with the structure of different salt-bearing inverted basins, such as the eastern part of the Parentis Basin or the Cameros Basin, where arching, uplift, and squeezing have been identified using seismic data.

The models and their restorations indicate that 2D and 3D changes in salt thicknesses and salt dispositions must be taken into account when interpreting these complex hanging-wall and salt structures in the extensional and inverted salt-bearing basins.

Acknowledgments

This research is part of the first author's Ph.D. thesis and has been supported by the SALTECRES (CGL2014-54118-C2-1-R MINECO/FEDER, UE) project and the Group of Geodynamics and Basin Analysis (2014SGR-467). The analog experiments were funded by the STAR Research Consortium, sponsored by the BG Group, BHPBilliton, ConocoPhilips, Eni, MarathonOil, Nexen, Shell, Talisman Energy, and YFP. We also thank K. D´Souza, J. Morris, and F. Lehane for logistical support in the modeling laboratory. The authors wish to thank Midland Valley Exploration Ltd. for providing academic licenses for the software Move used in the restoration of the cross sections. Reviews and suggested improvements by T. Dooley, O. Duffy, and S. Tavani were greatly appreciated. We are thankful for the English editing by G. G. Buffett.

References

Alves, T. M., R. L. Gawthorpe, D. W. Hunt, and J. H. Monteiro, 2002, Jurassic tectono-sedimentary evolution of the Northern Lusitanian Basin (offshore Portugal): Marine and Petroleum Geology, **19**, 727–754, doi: 10.1016/S0264-8172(02)00036-3.

Balkwill, H. R., and F. D. Legall, 1989, Whale Basin, offshore Newfoundland: Extension and salt diapirism. Extensional tectonics and stratigraphy of the North Atlantic Margins: AAPG Memoir, **46**, 233–246.

Benedicto, A., M. Séguret, and P. Labaume, 1999, Interaction between faulting, drainage and sedimentation in extensional hanging-wall syncline basins: Examples of Oligocene Matelles basin (Gulf of Lion rifted margin, SE France), *in* B. Duran, L. Jolivet, F. Horváth, and M. Séranne, eds., The mediterranean basins: Tertiary extension within the Alpine Orogen: Geological Society of London, Special Publications, 81–108, doi: 10.1144/GSL.SP.1999.156.01.06.

Buchanan, P. G., and K. R. McClay, 1991, Sandbox experiments of inverted listric and planar fault Systems: Tectonophysics, **188**, 97–115, doi: 10.1016/0040-1951(91)90317-L.

Burberry, C. M., 2015, Spatial and temporal variation in penetrative strain during compression: Insights from analog models: Lithosphere, **7**, 611–624, doi: 10.1130/L454.1.

Callot, J. P., J. F. Salel, J. Letouzey, J. M. Daniel, and J. C. Ringenbach, 2016, 3D evolution of salt controlled minibasins: Interactions, folding and megaflap development: AAPG Bulletin, **20**, 160–518, doi: 10.1306/03101614087.

Carola, E., J. A. Muñoz, and E. Roca, 2015,The transition from thick-skinned to thin-skinned tectonics in the Basque-Cantabrian Pyrenees: The Burgalesa Platform and surroundings: International Journal of Earth Sciences, **104**, 2215–2239, doi: 10.1007/s00531-015-1177-z.

Casas, J. M., J. D. Durney, J. Ferret, and J. A. Muñoz, 1996, Determinación de la deformación finita en la vertiente sur del Pirineo oriental a lo largo de la transversal del rio Ter: Geogaceta, **20**, 803–805.

Coward, M., and S. Stewart, 1995, Salt-influenced structures in the Mesozoic-Tertiary cover of the Southern North Sea, UK, *in* M. P. A. Jackson, D. G. Roberts, and S. Snelson, eds., Salt tectonics: A global perspective: AAPG, 229–250.

Coward, M. P., 1995, Structural and tectonic setting of the Permo-Triassic basins of northwest Europe: Geological Society of London, Special Publications, 7–39.

Dahlstrom, C. D. A., 1969, Balanced cross sections: Canadian Journal of Earth Sciences, **6**, 743–757, doi: 10.1139/e69-069.

Dercourt, J., L. E. Ricou, and B. Vrielynck, 1993, Atlas tethys palaeoenvironmental maps: Gauthier-Villars.

Dooley, T. P., M. P. A. Jackson, C. A. L. Jackson, M. R. Hudec, and C. R. Rodriguez, 2015, Enigmatic structures within salt walls of the Santos Basin — Part 2: Mechanical explanation from physical modeling: Journal of Structural Geology, **75**, 163–187, doi: 10.1016/j.jsg.2015.01.009.

Dooley, T. P., K. R. McClay, M. Hempton, and D. Smit, 2005, Salt tectonics above complex basement extensional fault systems: Results from analogue modelling, *in* A. G. Dore and B. A. Vining, eds., Petroleum geology: North-west Europe and global perspectives: Proceedings of the 6th Petroleum Geology Conference: Petroleum Geology Conferences Ltd. and the Geological Society, 1631–1648, doi: 10.1144/0061631.

Durcanin, M. A., 2009, Influence of synrift salt on rift-basin development: Application to the Orpheus Basin, offshore Canada: M.S. thesis, The State University of New Jersey.

Eisenstadt, G., and D. Sims, 2005, Evaluating sand and clay models: Do rheological differences matter?: Journal of Structural Geology, **27**, 1399–1412, doi: 10.1016/j.jsg.2005.04.010.

Ellis, P. G., and K. R. McClay, 1988, Listric extensional fault system-results of analogue model experiments: Basin Research, **1**, 55–70, doi: 10.1111/j.1365-2117.1988.tb00005.x.

Ferrer, O., 2012, Salt tectonics in the Parentis Basin (Eastern Bay of Biscay): Origin and Kinematics of salt structures in a hyperextended margin affected by subsequent contractional deformation: M.S. thesis, Universitat de Barcelona.

Ferrer, O., M. P. A. Jackson, E. Roca, and M. Rubinat, 2012, Evolution of salt structures during extension and inversion of the Offshore Parentis Basin (Eastern Bay of Biscay), *in* G. I. Alsop, S. G. Archer, A. J. Hartley, N. T. Grant, and R. Hodgkinson, eds., Salt tectonics, sediments and prospectivity: Geological Society of London, Special Publications, 361–380, doi: 10.1144/SP363.16.

Ferrer, O., K. R. McClay, and N. C. Sellier, 2016, Influence of fault geometries and mechanical anisotropies on the growth and inversion of hangingwall synclinal basins: Insights from sandbox models and natural examples, *in* C. Child, R. E. Holdsworth, C. A. L. Jackson, T. Manzocchi, J. J. Walsh, and G. Yieldings, eds., The geometry and growth of normal faults: Geological Society of London, Special Publications, 439, doi: 10.1144/SP439.8.

Ferrer, O., E. Roca, and B. C. Vendeville, 2008, Influence of a syntectonic viscous salt layer on the structural evolution of extensional kinked-fault systems: Bollettino di Geofisica Teorica ed Applicata, **49**, 371–375.

Ferrer, O., E. Roca, and B. C. Vendeville, 2014, The role of salt layers in the hangingwall deformation of kinked-planar extensional faults: Insights from 3D analogue models and comparison with the Parentis Basin: Tectonophysics, **636**, 338–350, doi: 10.1016/j.tecto.2014.09.013.

Glennie, K. W., 1995, Permian and Triassic rifting in northwest Europe: Geological Society of London, Special Publications, 1–5.

Groshong, R. H., Jr., C. Bond, A. Gibbs, R. Ratliff, and D. V. Wiltschko, 2012, Preface: Structural balancing at the

start of the 21st century: 100 years since Chamberlin: Journal of Structural Geology, **41**, 1–5, doi: 10.1016/j.jsg.2012.03.010.

Guimerà, J., Á. Alonso, and J. R. Mas, 1995, Inversion of an extensional-ramp basin by a newly formed thrust: The Cameros basin (N. Spain): Geological Society of London, Special Publications, 433–453.

Horsfield, W. T., 1977, An experimental approach to basement controlled faulting: Geologie en Mijnbouw, **56**, 363–370.

Hubbert, M. K., 1937, Theory of scaled models as applied to the study of geological structures: Geological Society of America Bulletin, **48**, 1459–1520, doi: 10.1130/GSAB-48-1459.

Hudec, M. R., and M. P. A. Jackson, 2007, Terra infirma: Understanding salt tectonics: Earth Science Reviews, **82**, 1–28, doi: 10.1016/j.earscirev.2007.01.001.

Hudec, M. R., M. P. A. Jackson, and D. D. Schultz-Ela, 2009, The paradox of minibasin subsidence into salt: Clues to the evolution of crustal basins: Geological Society of America Bulletin, **121**, 201–221, doi: 10.1130/B26275.1.

Huiqi, L., K. R. McClay, and D. Powell, 1992, Physical models of thrusts wedges, *in* K. R. McClay, ed., Thrust tectonics: Chapman and Hall, 71–81.

Jackson, M. P. A., C. Cramez, and J. M. Fonck, 2000, Role of subaerial volcanic rocks and mantle plumes in creation of South Atlantic margins: Implications for salt tectonics and source rocks: Marine and Petroleum Geology, **17**, 477–498, doi: 10.1016/S0264-8172(00)00006-4.

Jackson, M. P. A., and M. R. Hudec, 2017, Salt tectonics: Principles and practice: Cambridge University Press.

Jackson, M. P. A., D. D. Schultz-Ela, M. R. Hudec, I. A. Watson, and M. L. Porter, 1998, Structure and evolution of Upheaval Dome: A pinched-off salt diapir: Geological Society of America Bulletin, **110**, 1547–1573, doi: 10.1130/0016-7606(1998)110<1547:SAEOUD>2.3.CO;2.

Jackson, M. P. A., and C. J. Talbot, 1991, A glossary of salt tectonics: Bureau of Economic Geology.

Jackson, M. P. A., and B. C. Vendeville, 1994, Regional extension as a geologic trigger for diapirism: Geological Society of America Bulletin, **106**, 57–73, doi: 10.1130/0016-7606(1994)106<0057:REAAGT>2.3.CO;2.

Kehle, R. O., 1988, The origin of salt structures, *in* B. C. Schreiber, ed., Evaporites and hydrocarbons: Columbia University Press, 345–403.

Konstantinovskaya, E., and J. Malavieille, 2011, Thrust wedges with décollement levels and syntectonic erosion: A view from analog models: Tectonophysics, **502**, 336–350, doi: 10.1016/j.tecto.2011.01.020.

Koyi, H., M. K. Jenyon, and K. Petersen, 1993, The effect of basement faulting on diapirism: Journal of Petroleum Geology, **16**, 285–312, doi: 10.1111/j.1747-5457.1993.tb00339.x.

Koyi, H., and K. Petersen, 1993, Influence of basement faults on the development of salt structures in the Danish Basin: Marine and Petroleum Geology, **10**, 82–94, doi: 10.1016/0264-8172(93)90015-K.

Koyi, H. A., 2000, Towards dynamic restoration of geologic profiles: Some lessons from analogue modeling, *in* W. Mohriak and M. Taiwani, eds., Atlantic rifts and continental margins: American Geophysical Union, Geophysical Monograph Series 115, 317–329, doi: 10.1029/GM115p0317.

Koyi, H. A., and M. Sans, 2006, Deformation transfer in viscous detachments: Comparison of sandbox models to the South Pyrenean Triangle Zone: Geological Society of London, Special Publications, 117–134, doi: 10.1144/GSL.SP.2006.253.01.06.

Lingrey, S., and O. Vidal-Royo, 2015, Evaluating the quality of bed length and area balance in 2D structural restorations: Interpretation, **3**, no. 4, SAA133–SAA160, doi: 10.1190/INT-2015-0126.1.

Mathieu, C., 1986, Histoire géologique du sous-bassin de Parentis: Bulletin des Centres Recherche Exploration-Production Elf-Aquitaine, **10**, 22–47.

McClay, K. R., 1989, Analogue models of inversion tectonics: Geological Society of London, Special Publications, 41–59, doi: 10.1144/GSL.SP.1989.044.01.04.

McClay, K. R., 1990, Extensional fault systems in sedimentary basins: A review of analogue model studies: Marine and Petroleum Geology, **7**, 206–233, doi: 10.1016/0264-8172(90)90001-W.

Muñoz, J. A., 1992, Evolution of a continental collision belt: ECORS-Pyrenees crustal balanced cross-section, *in* K. R. McClay, ed., Thrust tectonics: Chapman and Hall, 235–246.

Nalpas, T., and J. P. Brun, 1993, Salt flow and diapirism related to extension at crustal scale: Tectonophysics, **228**, 349–362, doi: 10.1016/0040-1951(93)90348-N.

Nalpas, T., S. Le Douran, J. P. Brun, P. Untrnehr, and J. P. Richert, 1995, Inversion of the broad fourteens basin (offshore Netherlands): A small-scale model investigation: Sedimentary Geology, **95**, 237–250, doi: 10.1016/0037-0738(94)00113-9.

Ori, G. G., and P. F. Friend, 1984, Sedimentary basins formed and carried piggyback on active thrust sheets: Geology, **12**, 475–478, doi: 10.1130/0091-7613(1984)12<475:SBFACP>2.0.CO;2.

Rasmussen, E. S., S. Lomholt, C. Andersen, and O. V. Vejbæk, 1998, Aspects of the structural evolution of the Lusitanian Basin in Portugal and the shelf and slope area offshore Portugal: Tectonophysics, **300**, 199–225, doi: 10.1016/S0040-1951(98)00241-8.

Richardson, N. J., J. R. Underhill, and G. Lewis, 2005, The role of evaporite mobility in modifying subsidence patterns during normal fault growth and linkage, Halten Terrace, Mid-Norway: Basin Research, **17**, 203–223, doi: 10.1111/j.1365-2117.2005.00250.x.

Roure, F., J. O. Brun, B. Colletta, and J. Van Den Driessche, 1992, Geometry and kinematics of extensional structures in the Alpine foreland basin of southeastern

France: Journal of Structural Geology, **14**, 503–519, doi: 10.1016/0191-8141(92)90153-N.

Rowan, M. G., 2014, Passive-margin salt basins: Hyperextension, evaporite deposition, and salt tectonics: Basin Research, **26**, 154–182, doi: 10.1111/bre.12043.

Rowan, M. G., M. P. A. Jackson, and B. D. Trudgill, 1999, Salt-related fault families and fault welds in the northern Gulf of Mexico: AAPG Bulletin, **83**, 1454–1484.

Rowan, M. G., and B. C. Vendeville, 2006, Foldbelts with early salt withdrawal and diapirism: Physical model and examples from the northern Gulf of Mexico and the Flinders Ranges, Australia: Marine and Petroleum Geology, **23**, 871–891, doi: 10.1016/j.marpetgeo.2006.08.003.

Schellart, W. P., 2000, Shear test results for cohesion and friction coefficients for different granular materials: Scaling implications for their usage in analogue modeling: Tectonophysics, **324**, 1–16, doi: 10.1016/S0040-1951(00)00111-6.

Stapel, G., S. Cloetingh, and B. Pronk, 1996, Quantitative subsidence analysis of the Mesozoic evolution of the Lusitanian basin (western Iberian margin): Tectonophysics, **266**, 493–507, doi: 10.1016/S0040-1951(96)00203-X.

Stewart, S. A., and J. A. Clark, 1999, Impact of salt on the structure of the Central North Sea hydrocarbon fairways: Geological Society of London,Petroleum Geology Conference Series, 179–200.

Soto, R., M. Casas-Sainz, and P. Del Río, 2007, Geometry of half-grabens containing a mid-level viscous décollement: Basin Research, **19**, 437–450, doi: 10.1111/j.1365-2117.2007.00328.x.

Tankard, A. J., H. J. Welsink, and W. A. M. Jenkins, 1989, Structural styles and stratigraphy of the Jeanne d'Arc Basin, Grand Banks of Newfoundland. Extensional tectonics and stratigraphy of the North Atlantic margins: AAPG Memoir, **46**, 265–282.

Tavani, S., E. Carola, P. Granado, A. Quintà, and J. A. Muñoz, 2013, Transpressive inversion of a Mesozoic extensional forced fold system with an intermediate décollement level in the Basque-Cantabrian Basin (Spain): Tectonics, **32**, 146–158, doi: 10.1002/tect.v32.2.

Tavani, S., and P. Granado, 2014, Along-strike evolution of folding, stretching and breaching of supra-salt strata in the Plataforma Burgalesa extensional forced fold system (northern Spain): Basin Research, **27**, 573–585, doi: 10.1111/bre.12089.

Tugend, J., G. Manatschal, N. J. Kusznir, E. Masini, G. Mohn, and I. Thinon, 2014, Formation and deformation of hyperextended rift systems: Insights from rift domain mapping in the Bay of Biscay-Pyrenees: Tectonics, **33**, 1239–1276, doi: 10.1002/2014TC003529.

Vendeville, B., 1987, Champs de failles et tectonique en extension: Modélisation expérimentale: M.S. thesis, Université de Rennes.

Vendeville, B., 1988, Modèles expérimentaux de fracturation de lat couverture controlée par des failles normales dans le socle: Comptes Rendus Académie des Sciences Paris, **307**, 1013–1019.

Vendeville, B. C., H. Ge, and M. P. A. Jackson, 1995, Scale models of salt tectonics during basement-involved extension: Petroleum Geoscience, **1**, 179–183, doi: 10.1144/petgeo.1.2.179.

Weijermars, R., 1986, Flow behavior and physical chemistry of bouncing putties and related polymers in view of tectonic laboratory applications: Tectonophysics, **124**, 325–358, doi: 10.1016/0040-1951(86)90208-8..

Withjack, M. O., and S. Callaway, 2000, Active normal faulting beneath a salt layer: An experimental study of deformation patterns in the cover sequence: AAPG Bulletin, **84**, 627–651.

Withjack, M. O., and R. W. Schlische, 2005, A review of tectonic events on the passive margin of eastern North America, *in* P. Post, ed., Petroleum systems of divergent continental margin basins: 25th Bob S. Perkins Research Conference, Gulf Coast Section of SEPM, 203–235.

Yamada, Y., and K. R. McClay, 2003, Application of geometric models to inverted listric fault systems in sandbox experiments. Paper 1: 2D hanging wall deformation and section restoration: Journal of Structural Geology, **25**, 1551–1560, doi: 10.1016/S0191-8141(02)00181-5.

Ziegler, P. A., 1988, Evolution of the Arctic-North Atlantic and the Western Tethys: A visual presentation of a series of paleogeographic-paleotectonic maps: AAPG Memoir, **43**, 164–196.

Maria Roma received a B.S. (2012) in geology and an M.S. (2013) in reservoir geology and geophysics from the University of Barcelona. During her Ph.D., she did a research internship (2014) at the Fault Dynamics Research Group (Royal Holloway University of London). In 2015, she built up the analog modeling laboratory at the University of Dodoma, and she gave lessons in the M.S. petroleum geosciences division at the University of Dodoma. She now is pursuing a Ph.D. supported by an APIF predoctoral grant from the University of Barcelona, about the formation and inversion of extensional basins with syncline geometries in GEOMODELS Research Institute at the University of Barcelona.

Oskar Vidal-Royo received an M.S. (hons; 2006) in exploration, analysis, and modeling of basins and orogenic systems and a Ph.D. (high hons; 2010) in earth sciences from the University of Barcelona. After eight years with GGAC and the Geomodels Research Institute at the University of Barcelona, he joined Midland Valley Exploration in early 2013, working as a structural geologist carrying out consultancy, training, and research tasks for

oil and gas, mining, and carbon storage companies worldwide. In 2016, he cofounded Terractiva to deliver geologic consulting and advice for the hydrocarbon and mining industries at the regional, basin, and prospect/deposit scales. His research interests include seismic interpretation of complex structural styles, kinematic and geomechanical modeling of geologic bodies in two and three dimensions, salt tectonics, and tectonosedimentary relationships guiding fold-and-fault kinematics.

Ken R. McClay received a B.S. (honors) and D.S. from Adelaide University and an M.S. and Ph.D. from Imperial College, London. He is a professor of structural geology and the director of the Fault Dynamics Research Group at Royal Holloway University of London. His research has focused upon the dynamics of inverted, extensional, and strike-slip terrains and fault systems in fold-thrust belts. This involves the integration of field studies, seismic interpretation, and scaled physical modeling to develop quantitative 4D models for fault systems in sedimentary basins.

Oriol Ferrer received a B.S. and a Ph.D. in earth sciences from the University of Barcelona. He also did a postdoc at the Fault Dynamics Research Group (Royal Holloway University of London). Since 2010, he has been in charge of the GEOMODELS Analog Modeling Laboratory, UB. He is a tenured lecturer at UB. His research interests include salt tectonics of rift systems, inverted basins, and salt-bearing passive margins using outcrop, subsurface, and analog modeling.

Josep Anton Muñoz received a Ph.D. (1985) from the University of Barcelona and worked for the Servei Geologic de Catalunya from 1985 to 1990, when he joined the University of Barcelona. He is a professor of structural geology at UB. He is the director of the GEOMODELS Research Institute. His research interests include the structure of thrust-and-fold belts, tectonosedimentary relationships, tectonics of collisional orogens, and construction of 3D structural models.